



## Modeling of land subsidence due to groundwater overexploitation using elastoplastic Mohr-Coulomb model in Arak plain, Iran

Mohammad Hossein Jahangir\*, Zahra Khosravi, Hamid Sarrafha

Department of environment and renewable energies, Faculty of new sciences & technologies, University of Tehran, Tehran, Iran

Received: 14 December 2019, Revised: 08 July 2020, Accepted: 24 August 2020

© University of Tehran

### Abstract

Land subsidence due to groundwater overexploitation has been considered among the natural hazards for the last decades. Accordingly, a growing global concern has been forwarded towards this issue regarding its measurement, prediction, and prevention. In addition to measurement techniques, mathematical and numerical methods could be used for subsidence modelling and its prediction via appropriate software tools and modelling frameworks. As a part of the global trend, groundwater overexploitation and the subsequent land subsidence has lately become a major environmental threat in Iran. In this paper, the land subsidence across Arak plain, a relatively vast plain located in central Iran, caused by groundwater level drop is calculated using Mohr-Coulomb elastoplastic model, which is a structural soil modelling framework. Also, a modified finite element method is applied via PLAXIS 2D commercial software for acquiring further insight and verifying the results from the Mohr-Coulomb model. Accordingly, five borehole stations were considered across the Arak plain, namely Gavkhaneh, Ebrahimabad, Safarabad, Amanabad, and MojedabadKohneh and the mentioned model is applied at each borehole. It was revealed that the axial strain across the plain has reached extreme negative value of -0.190 in 2014, which shows severe soil compaction. Also, the volumetric strain rate reached a minimum value of -0.083 in 2014. The acquired results from the applied Mohr-Coulomb model showed a subsidence average value of 26.6 cm for 17.85 m of groundwater level drop during 1991-2014. Also, the lowest aggregated subsidence value until 2014 was observed at Safarabad station being 0.2 cm, while its maximum value was observed at Gavkhaneh station being 88.75 cm. These was a 9.20% of difference between the average value acquired by Mohr-Coulomb model and FEM, which, considering the uncertainty in measured input data verifies the reliability of the model. The research findings prove the capability of the Mohr-Coulomb model in modelling land subsidence.

**Keywords:** Subsidence, Numerical modeling, Elastoplastic Mohr-Coulomb Model, Underground Water Level, Iran

### Introduction

Land subsidence is a major threat in areas with high rates of groundwater exploitation. These areas mostly include lands with agricultural utility, lands close to deltas and seas, and highly populated regions (G Gambolati & Teatini, 2015). The threat becomes more noteworthy when the global warming is taken into account, turning flooding into a likely consequence of land subsidence. In recent years, land subsidence caused by ground water overexploitation has been reported in various regions and countries across the world. It is usually evaluated over large areas for a relatively long periods of time using geodesy and satellite imagery by monitoring vertical land movements as well as using extensometers (Koster et al., 2016). Also, various numerical techniques are used for predicting its pattern in the future.

\* Corresponding author e-mail: mh.jahangir@ut.ac.ir

Throughout the world, land subsidence has been reported in Shanghai delta, China (Chai et al., 2004), Jakarta, Indonesia (Abidin et al., 2001), Cerro Prieto geothermal field, Baja California, Mexico (Carnec & Fabriol, 1999), Lost Hills and Belridge oilfields, California (Fielding et al., 1998), Romagna region, Italy (Giuseppe Gambolati et al., 1999; Teatini et al., 2006), Atlantic coast of north America (Karegar et al., 2016), Yellow River delta, China (Higgins et al., 2013), Hangzhou-Jiaxing-Huzhou Plain, China (Changjiang Li et al., 2006), northern Gulf of Mexico (Kolker et al., 2011), Mexico city (Ortega-Guerrero et al., 1999; Ortiz-Zamora & Ortega-Guerrero, 2010), Bangkok, Thailand (Phien-wej et al., 2006), central Mexico (Chaussard et al., 2014), northern Beijing plain, China (Hu et al., 2004; Zhu et al., 2015), Alexandria, Egypt (Wöppelmann et al., 2013), Yunlin County of central Taiwan (Tung & Hu, 2012), Semarang, Indonesia (Lubis et al., 2011; Marfai & King, 2007) greater Cairo, Egypt (Aly et al., 2009), Houston, Texas (Buckley et al., 2003) (Buckley et al., 2003), and South-central and Southern Arizona, USA (Conway, 2015) among others. In Iran, land subsidence has become a major environmental threat recently due to unregulated underground water exploitation, mostly for agricultural purposes. It has been reported in Tehran basin (Alipour et al., 2008; Dehghani et al., 2013; Mahmoudpour et al., 2016), Rafsanjan (Sayyaf et al., 2014), Mashhad valley (Motagh et al., 2007), Kashmar valley (Anderssohn et al., 2008), and Neyshabour (Dehghani et al., 2009).

There are various subsidence evaluation and measurement methods available. In general, the experimental evaluation methods could be classified into two categories of ground based geodetic techniques and remotely-sensed geodetic techniques (Galloway & Burbey, 2011). As for the first category, the precise differential leveling is selected in cases where vertical position is the only requirement. When the survey length is small (10 kilometers or less), differential leveling is still preferred, since it is accurate as well as economical (Galloway & Burbey, 2011). However, first order accuracy leveling is not easy to perform by this method and requires satellite based GPS. Also, extensometry could be utilized in cases where precise evaluation values are required at local scale. As another method in this category, Tripod light detection and ranging (T-LiDAR) could be mentioned. Remotely sensed geodetic techniques include InSAR and LiDAR, among others (Galloway & Burbey, 2011).

Land subsidence could also be estimated and modeled via numerical methods. This strategy is specifically useful when a future trend prediction is required. Several attempts are found in the literature in this field. Zhou et al. (Zhou et al., 2010) used a three-dimensional finite difference method to evaluate the subsidence accompanied by a foundation dewatering project in Shanghai, China. Larson et al. (Larson et al., 2001) predicted the optimal safe groundwater extraction levels for preventing land subsidence in Los Banos-Kettleman City area, California. They used an integrated groundwater and subsidence simulation model and proposed the necessary predictive measures. Wu et al. (Wu et al., 2009) utilized a 3D finite element model to simulate the land subsidence across Su-Xi-Chang area, China caused by groundwater overexploitation. Ye et al. (Ye et al., 2016) conducted a three-dimensional land subsidence modeling in downtown Shanghai for a 16 year period. They calibrated their model using piezometric, geodetic-leveling, and borehole extensometer evaluations performed throughout the simulation period. Stress-strain as well as moisture transfer in porous media models are excessively useful for subsidence simulation. Krejci et al. (Krejci et al., 2013) presented a coupled hydro-mechanical numerical model for simulating soil behavior. They based their model on effective stress concept. Calderhead et al. (Calderhead et al., 2011) simulated land subsidence induced by pumping in the Toluca Valley, Mexico. They applied Terzaghi's 1D instantaneous compaction principle along with a 3D groundwater flow model. After that they used the D-InSAR measurement tool as well as extensometers to validate the acquired results.

Li and Liu (Chao Li & Liu, 2014) evaluated the subsidence mechanisms of the Songliao basin, China. They utilized backstripping as well as strain rate inversion method and analyzed

20 boreholes for this purpose. Jin et al. (Jin et al., 2016) performed the sensitivity analysis on the parameters involved in land subsidence simulation due to groundwater overexploitation. Yang et al. (Yang et al., 2015) applied Galerkin finite element model on hydraulic properties of land subsidence and verified their model by the known analytical solutions in the confined aquifer. Shearer (Shearer, 1998) developed a numerical computer code for the MODFLOW model to calculate the subsidence at Hangu, China. Zhang et al. (Zhang et al., 2018) investigated the pumping induced stress-strain rates in aquifer systems of Wuxi, China. They showed that a considerable area on the ground surface gets under tensile strain due to pumping. Xu et al. (Xu et al., 2018) incorporated backstripping, modified strain-rate inversion as well as revised finite extension modelling methods to evaluate the pattern and origin of subsidence in the Dongpu Sag, in the Bohai Bay Basin, northeast China. Finally as a case in Iran, Sayyaf et al. (Sayyaf et al., 2014) simulated the land subsidence across Rafsanjan plain using a 2D finite element model. They showed that if the exploitation rate remains constant in the upcoming years, the land settlement would reach a high value of 110 cm by 2022.

As a recent case study in Iran, Taravatrooy et al. (Taravatrooy et al., 2018) employed a hybrid clustering-fusion method for subsidence estimation of Tehran province. Their method comprised genetic algorithm for optimization, k-means method, and multiple soft computing models for additional accuracy. They used five soft computing models with hydrogeological forcing of frequency and thickness of fine-grained sediments, groundwater depth, water level decline, transmissivity and storage coefficient, and land subsidence rate. In another recent attempt, Ghorbanzadeh et al. (Ghorbanzadeh et al., 2018) predicted the land subsidence of Marand plain, northwest Iran, utilizing an adaptive neuro-fuzzy inference system (ANFIS) employing six membership functions. They further combined the developed predictive model with geographical information system (GIS) for subsidence susceptibility mapping across the region. According to the authors, combining ANFIS with GIS data layers could yield susceptibility mapping with high accuracy. Dehghani and Nikoo (Dehghani & Nikoo, 2019) calculated approximate subsidence rate of three regions in Iran, namely Varamin, Neyshabour, and Shahriar plains reporting maximum subsidence values of 0.4 m/year, 0.16 m/year, and 0.25 m/year, respectively. They conducted their research on three mentioned case studies using SAR interferometry and persistent scatterer interferometry. The reported values prove the concerning state of Iran regarding land subsidence, which is mostly due to drought like climate conditions and groundwater overexploitation. Finally, Rajabi (Rajabi, 2018) numerically evaluated the subsidence of Aliabad plain, located in Qom, Iran using PLAXIS 3D software. To this end, he utilized aquifer pressure variations and hydrological as well as geotechnical data. He has found that during 2001-2013 period, 26.35 m of water level has declined in the region, which in turn has led to a maximum subsidence value of 76 cm throughout the area.

In this paper, the land subsidence due to groundwater exploitation is mathematically modeled via Mohr-Coulomb elastoplastic model for Arak plain. It is evident that measurement and experimental-bases methods for evaluating land subsidence could be expensive and require huge amounts of time and equipment. On the contrary, numerical and mathematical models could yield useful and reliable data on land subsidence for extensive time durations requiring less effort. In this regard, these models are beneficial when there is lack of data and measurement equipment or the aim is to predict the subsidence behavior in the future. Linear and non-linear elastic models could be used for modelling the loading and unloading within the soil medium caused by groundwater level variations. It is showed in this paper that the Mohr-Coulomb model could be used effectively for this purpose using limited number of soil parameters. Another major benefit of this model as compared to other models is its flexibility, which enables it to cover a vast variety of soil mediums with distinct characteristics and behavior. For completing and verifying the conducted analysis, a modified finite element method is also applied for subsidence calculation using PLAXIS 2D software. The acquired

results from the two conducted simulations are compared with each other and acceptable agreement is observed, further proving the validity of the Mohr-Coulomb model for land subsidence numerical evaluation.

### Plain specifications and modelling methodology

Arak plain has an area of approximately 5483 km<sup>2</sup> and is located in western Iran at eastern 18°:50′-20°:49′ of longitude and northern 44°:34′-49°:33′ of latitude. Fig. 1 shows the location of the Arak plain with respect to the country extracted from GIS. Furthermore, Fig. 2 depicts the geological map of Arak plain, within which the groundwater stream directions are determined. For the modelling, five borehole stations were selected across the plain, at which geotechnical as well as water level data were available. However, considering that the current research follows a numerical and modelling approach, the available data were enough to prove the applicability of the proposed model for subsidence prediction. The measurement boreholes were located at Amanabad, Ebrahimabad, Safarabad, Gavkhaneh, and Mojedabade-Kohneh. The investigation site included one primary aquifer in Arak plain and two subsidiary aquifers in Govar-Aghilabad and Tabarteh regions. Corresponding data were acquired from Iran water resources management company, regional water company of Markazi. Finally, Fig. 3 depicts the groundwater levels of Arak plain in 1991 and 2014. As observed from the figure, the groundwater stream is inversed at western and west-southern regions of the primary aquifer, due to overexploitation.

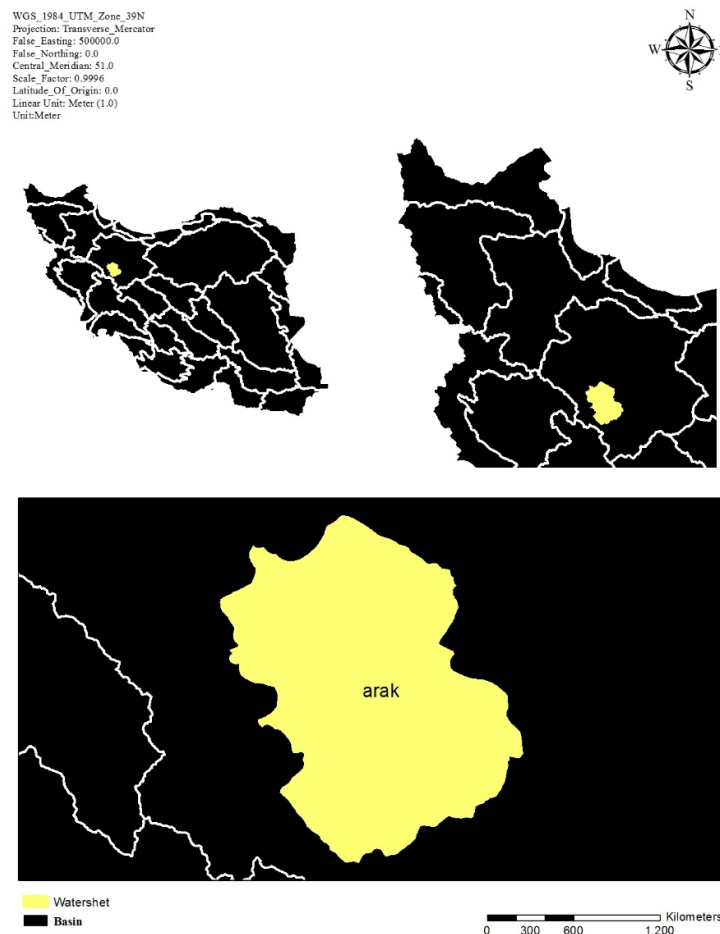


**Figure 1.** GIS extracted location of the Arak plain with respect to Iran

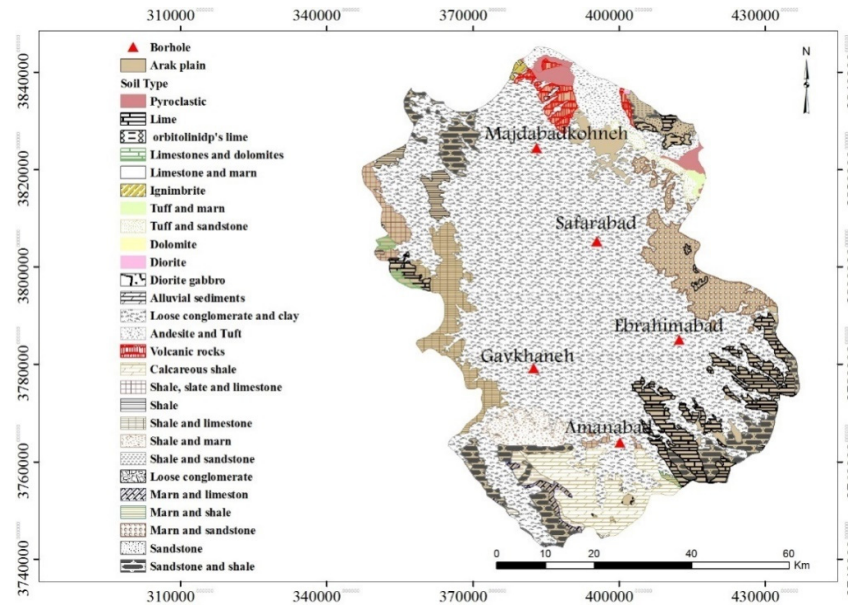


**Figure 2.** Geological map of the Arak plain located in Western Iran at eastern 18°:50′-20°:49′ of longitude and northern 44°:34′-49°:33′ of latitude

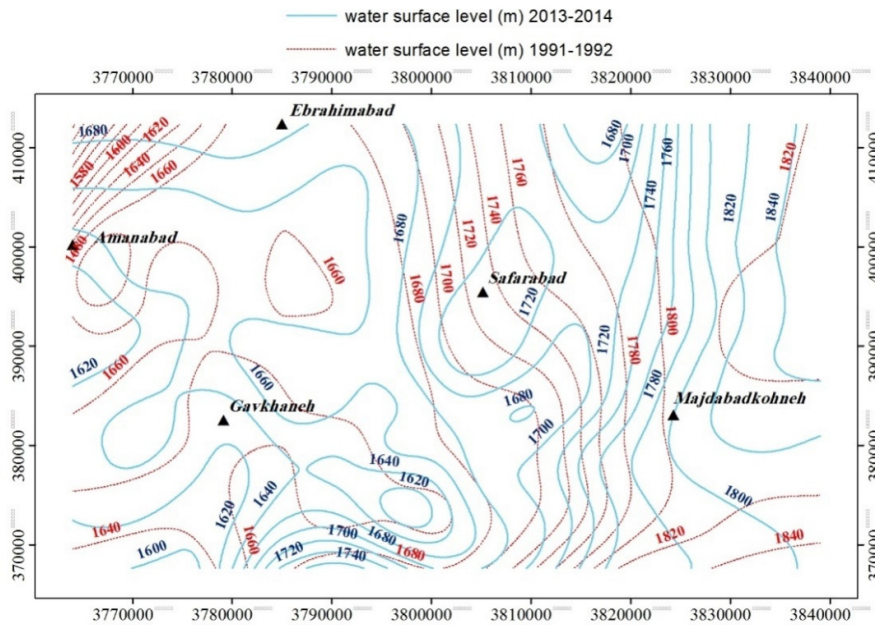


**Figure 3.** Groundwater levels of Arak plain in 1991 and 2014, data acquired from Iran water resources management company, regional water company of Markazi

In the present study, groundwater level variations data were acquired for each hydrological year during within 1991-2014. The values are reported in October which marks the start of the hydrological year. For providing further information, the corresponding values of groundwater level variations for each hydrological year are reported in Table A1 Appendix A. Due to different levels of precipitation and exploitation, the groundwater level behaves as a periodic function with respect to time in the region. This periodic trend leads to a cyclic loading mode. Positive values correspond to loading while negative values correspond to unloading state. The soil behavior was evaluated by calculating the variation of the soil's geotechnical

characteristics, which in turn were caused by groundwater level fluctuations. To this end, the elastoplastic Mohr-Coulomb model was employed for each measurement borehole at the first phase of the research. As the first step, the loading-unloading cycles were determined for each borehole. After that, the Mohr-Coulomb model parameters were calculated using the geotechnical as well as stratigraphic data of measurement boreholes, which are listed in Table 1. Utilized geotechnical parameters were soil cohesion for coarse-grain soil, and friction angle for fine-grain soil. These two parameters were used by the Mohr-Coulomb model for evaluating the shear strength of the soil. For the elastic state, the Young modulus ( $E$ ) as well as the Poisson coefficient ( $\nu$ ) were used in Hooke's law, as will be stated in equation (6) in the next section. The soil grain density ( $\gamma$ ) was also provided. The soil profiles of the stations are provided in Fig. 4 for better understanding of the boreholes' stratigraphic structure and their composing layers.

As the first phase of the research, Mohr-Coulomb model was implemented via computer coding in MATLAB. After evaluating the subsidence with Mohr-Coulomb model via self-coding, the land subsidence was calculated using PLAXIS 2D for further analysis and verification.

### Appendix A

**Table A1.** Groundwater level variations at selected boreholes, namely Amanabad, Ebrahimabad, Safarabad, Mojedabadekohne, and Gavkhaneh across the Arak plain during 1991-2014 hydrological years

Hydrological year	Groundwater level variation (m/year) for borehole stations				
	Amanabad	Ebrahimabad	Safarabad	Mojedabade kohneh	Gavkhaneh
1991-92	-1.8	0.6	0	0	0
1992-93	6.6	0.5	1	0	0
1993-94	-3.3	0	0.4	0	0
1994-95	1.2	0.7	-0.05	0	0
1995-96	1.3	0.1	1.65	0	0
1996-97	28.5	-0.9	0.6	0	0
1997-98	-4.2	-0.05	-0.05	0	0
1998-99	-2.6	-0.25	0	0	0
1999-2000	-0.1	0.2	0.15	0	0
2000-01	-7.24	1.58	-0.35	0	0
2001-02	0.23	0.47	0.62	-1.91	30.55
2002-03	-4.3	-0.03	-0.15	1.72	0
2003-04	-0.83	0.34	-0.36	4.33	-45.05
2004-05	-4.48	-0.91	-0.69	-2.6	3.07
2005-06	-1.15	-0.85	0.04	-3.32	-4.58
2006-07	-2.5	-0.4	-0.95	0.29	1.26
2007-08	-3.35	-1.0	0	-0.83	-2.05
2008-09	-3.0	0	-0.85	-0.77	-1.1
2009-10	-2.89	0	-1.03	-0.33	-2.25
2010-11	-0.98	0	2.9	0.6	-0.72
2011-12	-4.93	0	-0.54	-0.35	0.4
2012-13	-4.0	0	-1.64	-0.73	-5.15
2013-14	-1.8	0	-0.44	0.01	1.42

**Table 1.** Geotechnical data of the soil at the five measurement boreholes, data acquired from Iran water resources management company, regional water company of Markazi

Parameter	MojedabadKohne	Safarabad	Gavkhaneh	Ebrahimabad	Amanabad
E (kPa)	$3.04 \times 10^4$	$3.06 \times 10^4$	$3.09 \times 10^4$	$2.03 \times 10^4$	$2.42 \times 10^4$
C (kPa)	4.3	3.6	7.9	7.3	7.4
$\phi$ (°)	30.17	29.49	29.64	28.26	29.46
$\gamma$ (kg/m <sup>3</sup> )	18.1	18.3	18.2	17.8	17.5
$\nu$	0.259	0.256	0.263	0.246	0.245

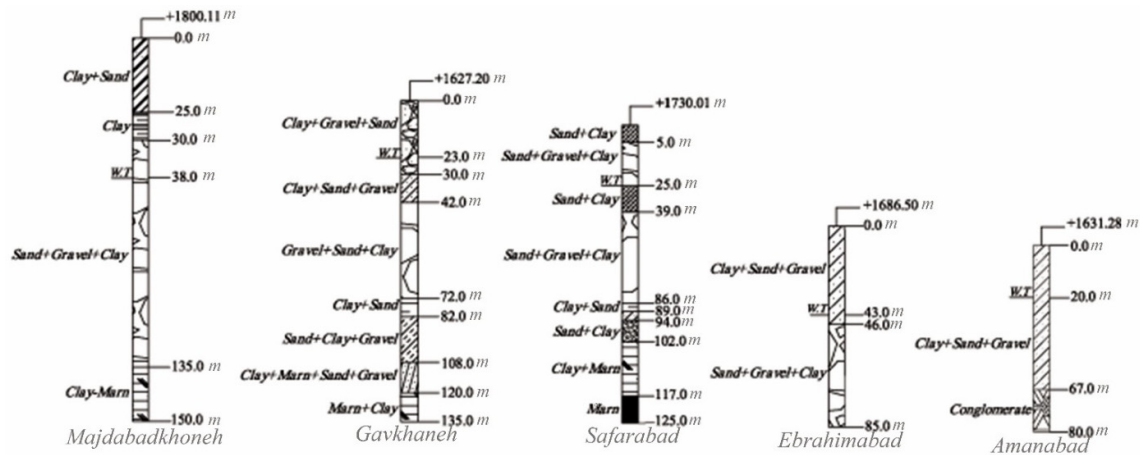


**Figure 4.** Soil profiles of investigation boreholes (in order from right Amanabad, EbrahimAbad, Safarabad, Gavkhaneh and Mojedabadkohneh), data acquired from Iran water resources management company, regional water company of Markazi

PLAXIS 2D is a two dimensional finite element-based commercial software commonly used for stress-strain calculations in various geotechnical applications. The geometry of the problem was first defined in the software, including the nodes, the physical model borders, soil layers, and soil's structural compositions. After that, exerted loads as well as the boundary conditions were determined for the program. Finally, the Mohr-Coulomb elastoplastic model was then selected as the soil's constitutive model. As will be stated in the next section, this model consists of five major parameters. These parameters include soil cohesion factor, external friction angle, Young's modulus, Poisson ratio, and dilation angle. In PLAXIS 2D modelling, a coarse mesh was used for initial calculations, which included 50 elements, and then a mesh was constructed on the defined soil geometry. After performing the finite element mesh, the initial water level was determined and the calculations started using initial underground water pressure. At this point the calculation phases were defined and the stress-strain values were calculated for each phase. These values were finally used for subsidence evaluation.

**Mohr-Coulomb elastoplastic model**

For the Mohr-Coulomb materials, the failure criterion function, denoted by  $F$ , depends upon material's intrinsic properties and is defined as follows:

$$F = \sigma_m \sin \phi + \sqrt{J'_2} \left( \cos \theta - \frac{1}{\sqrt{3}} \sin \theta \sin \phi \right) - c \cos \phi = 0 \tag{1}$$

in which  $\sigma_m$ ,  $\phi$ ,  $J'_2$ , and  $c$  represent the mean of the principal stresses, friction angle, second stress matrix invariant, and soil cohesion respectively, and  $\theta$  is calculated as follows:

$$\theta = \frac{1}{3} \sin^{-1} \left( -\frac{3\sqrt{3}}{2} \frac{J'_3}{J_2^{1.5}} \right), \quad -\frac{\pi}{6} < \theta < \frac{\pi}{6} \tag{2}$$

in which  $J'_3$  is the third stress matrix invariant.

The strain rate is calculated as follows based on the basic principle of plasticity:

$$\epsilon = \epsilon^e + \epsilon^p \tag{3}$$

in which  $\varepsilon$ ,  $\varepsilon^e$ , and  $\varepsilon^p$  denote the total, elastic, and plastic strain rates, respectively. Hooke's law expresses the elastic strain-stress relation as follows:

$$\sigma = \mathbf{D}^e \cdot \varepsilon^e = \mathbf{D}^e (\varepsilon - \varepsilon^p) \quad (4)$$

in which  $\mathbf{D}^e$  denotes the elastic stiffness matrix. In three dimensional cases, the plastic strain increase is expressed via a function,  $Q$ . Also, the elastoplastic strain rate could be estimated as follows:

$$\varepsilon = \mathbf{C}^{ep} \cdot \sigma = \mathbf{C}^e \cdot \sigma + \mathbf{C}^p \cdot \sigma = (\mathbf{C}^e + \mathbf{C}^p) \cdot \sigma \quad (5)$$

in which  $\mathbf{C}^e$ ,  $\mathbf{C}^p$ , and  $\mathbf{C}^{ep}$  represent the elastic, plastic, and elastoplastic softness matrices, respectively. In perpendicularity, the plastic strain is calculated as:

$$d\varepsilon^p = -\lambda \cdot \left( \frac{\partial Q}{\partial \sigma} \right) = \frac{\left( \frac{\partial F}{\partial \sigma} \right) \left( \frac{\partial Q}{\partial \sigma} \right)^T}{\left( \frac{\partial F}{\partial \varepsilon^p} \right)^T \left( \frac{\partial Q}{\partial \sigma} \right)} d\sigma \quad (6)$$

in which  $F$  and  $\lambda$  denote the yield surface and plasticity coefficient, respectively. If the stiffening coefficient would be defined as  $H = -\left( \frac{\partial F}{\partial \varepsilon^p} \right)^T \left( \frac{\partial Q}{\partial \sigma} \right)$ , the plastic strain matrix could be calculated as follows:

$$\mathbf{C}^p = \frac{1}{H} \left[ \frac{\partial F}{\partial \sigma_{ij}} \right] \left[ \frac{\partial Q}{\partial \sigma_{ij}} \right] \quad (7)$$

The presented relations were used for calculating axial as well as volumetric strain rates, which in turn were used for subsidence estimation for each station and over the whole plain. By exploiting underground water, increasing stress levels are exerted to the fine-grain layer of the local soil and consequently, the hydraulic pressure decreases, leading to unrecoverable soil compaction at the site. Overtime, the plastic deformation of the soil structure causes the soil layer pores to be filled and therefore, the soil experiences volumetric compaction. This ultimately leads to land subsidence. The resultant aggregated subsidence was estimated from the stress-strain as well as volumetric strain curves at each borehole using the following relation:

$$s_i = \varepsilon_i \times (h_w - \sum_{n=i}^{i+1} \varepsilon_n) \quad (8)$$

in which  $h_w$  and  $\varepsilon_i$  are the groundwater level and axial strain for the  $i$ th year, respectively.

## Results and discussions

In this section, the acquired results from the modelling and numerical analysis are presented and discussed. At first, the developed model is validated based on a related research on subsidence evaluation of Rafsanjan plain, Kerman, Iran (Sayyaf et al., 2014). After that, stress-strain curves as well as volumetric strain rates are calculated using the elastoplastic Mohr-Coulomb model. The land subsidence values are then calculated for each borehole station based

on the elaborated relation in the previous section. Finally, the acquired results from the PLAXIS 2D modelling are presented and elaborated.

### Model validation

The developed Mohr-Coulomb model is validated by comparing its results with a previously conducted analysis by Sayyaf et al. (Sayyaf et al., 2014) on Rafsanjan plain, Kerman, Iran in 2013. For this purpose, the geotechnical specifications of the Rafsanjan plain elaborated by Sayyaf et al. (Sayyaf et al., 2014) were inserted into the Mohr-Coulomb model utilized by the present paper. The acquired land subsidence value for the Rafsanjan plain by our model was then compared with that of (Sayyaf et al., 2014).

Considering the major structure of the Rafsanjan plain soil, the internal friction angle and soil cohesion factor were considered to be  $32^\circ$  and 10 kPa. In addition, other plain Geotechnical data were presented by Sayyaf et al. (Sayyaf et al., 2014), which are listed in Table 2.

Aggregated land subsidence across Rafsanjan plain during 1984-2009 was acquired to be 66.06 cm via the Mohr-Coulomb elastoplastic model developed in the current research effort. This is while this value has been acquired by Sayyaf et al. (Sayyaf et al., 2014) to be 70.00 cm, which shows 5.63% of difference between the results of the two efforts. This proves the acceptable validity of the Mohr-Coulomb elastoplastic model. It should be note that the mentioned difference could even be due to existing uncertainty in measuring the soil geotechnical and hydrological characteristics. Furthermore, Fig. 5 depicts the stress-strain curve for Point A borehole specified in (Sayyaf et al., 2014) in Rafsanjan plain which is calculated by our numerical model.

**Table 2.** Soil geotechnical data for Rafsanjan plain utilized in the Mohr-Coulomb model (Sayyaf et al., 2014).

Soil structure	Young's modulus, E (Pa)	Poisson ratio, $\nu$	Density, $\rho$ (kg/m <sup>3</sup> )	N
Sand and gravel	$20 \times 10^6$	0.25	2760	0.3
Clay and silt	$9 \times 10^6$	0.30	2760	0.4

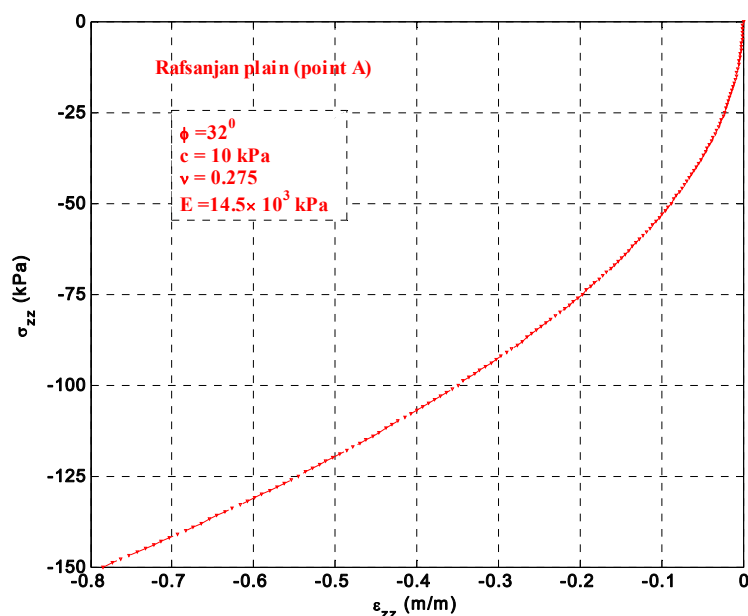


**Figure 5.** Stress-Strain curve for Point A borehole in Rafsanjan plain specified by Sayyaf et al. (Sayyaf et al., 2014) calculated by the Mohr-Coulomb model developed in the current research.

### Mohr-Coulomb model results

Fig. 6 shows the stress-strain curves versus time during 1991-2014 for Gavkhaneh and Amanabad stations, calculated using Mohr-Coulomb elastoplastic model. The Gavkhaneh station has undergone tensile stress load due to increasing underground water levels until 2001, reaching a maximum axial strain of 0.33 for 305 kPa of axial stress. From there, negative stress-strain values were obtained caused by continuous water overexploitation, leading to soil compaction. Due to reduced groundwater levels, the negative values of axial strain were obtained until 2014, reaching a level of about -0.47 for -240 kPa of axial stress. This indicates significant level of soil compaction. In case the ground water level drop has not been compensated by precipitation, it could be predicted that the same trend could have continued by now, which could have led to considerable soil compaction levels.

Similarly, the Amanabad station underwent tensile stress loads and consequently experienced soil inflation until 1996. It reached a maximum strain of 0.504 for 342 kPa of stress. From there, decreasing underground water levels led to negative stress loads, causing soil compaction. The site then experienced minimum value of axial strain of -0.344 for -115.7 kPa of axial stress. Although both sites have approximately similar soil cohesion and friction angles, higher stress-strain diagram slopes were observed for the Gavkhaneh station, which is due to higher Young's modulus of this site. This could be deduced from geotechnical values listed in Table 1.

Fig. 7 illustrates the soil volumetric strain rate for Gavkhaneh and Amanabad stations during 1991-2014. It is evident from the figure that Gavkhaneh station reached a maximum value of 0.17 of volumetric strain in 2011, while it ended up at -0.19 in 2014. Also, the Amanabad station reached a maximum volumetric strain value of 0.26 in 1998 and ended up at -0.16 in 2013. The overall trend of the volumetric stresses shows massive soil compaction. It is evident from the figure that Amanabad curve has a higher slope. The soil structure of Amanabad station is more silt-gravel based on acquired data from regional water company of Markazi. Due to having a coarse-grain structured soil, this station is more prone to soil compaction. This is because in coarse-grain soils like gravel, the aquifer is more likely to collapse when the water is extracted from its soil structure. Considering this fact, if the same trend has been continued over the previous years, higher subsidence values could be predicted for Amanabad station as compared to Gavkhaneh station.

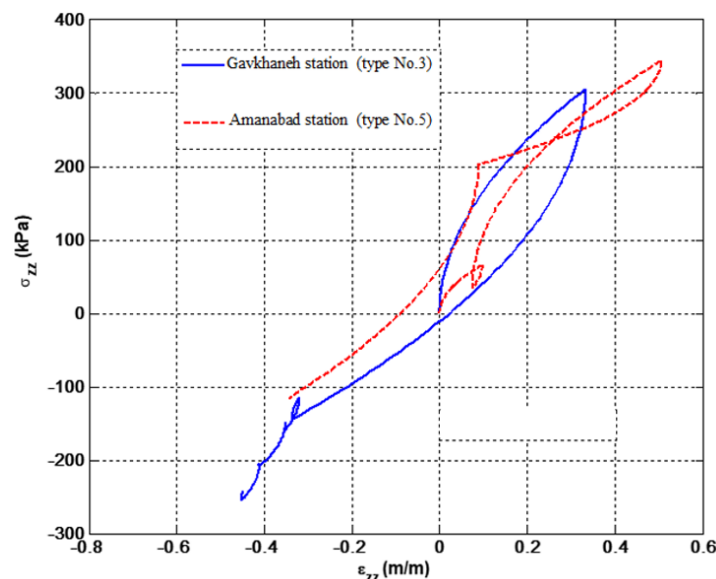


**Figure 6.** Stress-strain curves for Gavkhaneh and Amanabad stations during loading-unloading cycles within 1991-2014

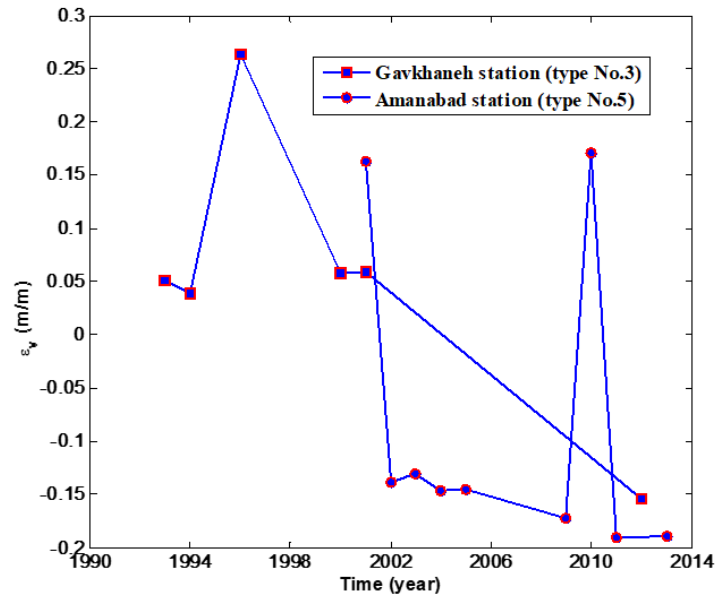


**Figure 7.** Volumetric strain rate curves for Gavkhaneh and Amanabad stations during 1991-2014

Fig. 8 depicts the stress-strain curves during the same time period for Ebrahimabad and Safarabad stations. It is observed from the figure that Ebrahimabad station underwent a cyclic pattern of underground water levels, experiencing soil inflation for the first loading cycle, soil compaction for the next, and then again soil inflation for the next cycle. During period under investigation, it reached a maximum value of 0.01687 in 2010. From there, serious soil compaction trend is recognizable from the figure, which continued until the end of the period. It reached a minimum value of approximately 0 in 2014. On the other hand, Safarabad station showed an approximately similar trend to Ebrahimabad station, with the exception of the curve slope, which is lower for Safarabad station. This is due to lower Young's modulus of this site compared to Ebrahimabad. In this sense, it could be claimed that this site is less prone to land subsidence in comparison. Safarabad station's axial strain rate reached a maximum value of 0.02 in 2001 and came down to a minimum of about 0 in 2014. If the same trend has been persisted, it could have experienced negative values for axial strain rate, pointing out to soil compaction.

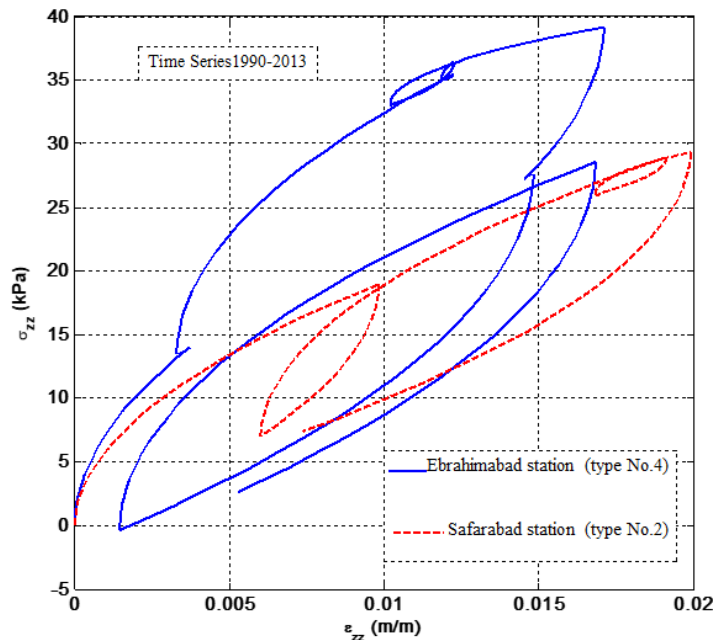
Fig. 9 shows the volumetric strain rate versus time diagram for Ebrahimabad and Safarabad stations during 1991-2014. It is seen in the figure that the Safarabad station reached a minimum value of 0.0011 and a maximum value of 0.0172. Also, the Ebrahimabad station reached a maximum value of 0.010 and a minimum value of 0.0033. It is clear from the figure that the Safarabad station's volumetric strain rate underwent more severe variations compared to that of Ebrahimabad station. Although the maximum volumetric strain rate variation values are close for the two mentioned stations, Ebrahimabad station has underwent more severe variations statistically. It could be deduced that the soil at Ebrahimabad station shows more severe reaction to exerted stresses and consequently, higher values of land subsidence could be predicted for this station in comparison. This phenomenon could also be justified geologically according to the soil structure of the stations. Since the soil is more coarse-grain more gravel-type at Ebrahimabad, the soil has higher hydraulic conductance making it more prone to compaction under equally exerted stresses.

Fig. 10 shows axial stress versus strain rate diagram for the MojedabadKohneh station. It is observed that for the first, third, and fourth loading-unloading cycles, soil inflation has occurred due to increased underground water levels. Consequently, the axial strain rate reached a maximum value of 0.065. From there, continuous lowering of the axial stress was observed,

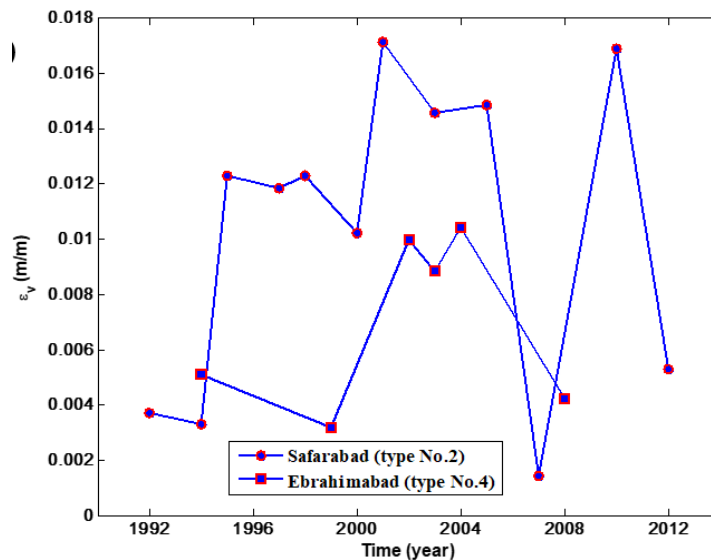
which showed severe reduction of underground water levels. The same trend continued until 2014, at which year the axial strain rate reached a minimum value of approximately 0. If the same trend has been continued over the past years, it could be predicted that the strain rate would have taken negative values after 2014.

Fig. 11 depicts the volumetric strain rate versus time for MojedabadKohneh station during 1991-2014. The soil compaction is completely visible, reaching a minimum value of 0.0026. However, high slopes of volumetric strain rate reduction is not predicted for this station during the upcoming years based on the status until 2014.

The main structural feature determining the stress-strain rate behavior of local soil at different boreholes is the soil's grain size. It is evident that larger soil grain sizes are more prone to soil compaction in case the structural water is depleted from local soil.



**Figure 8.** Stress-strain curves for Ebrahimabad and Safarabad stations during loading-unloading cycles within 1991-2014



**Figure 9.** Volumetric strain rate versus time for Ebrahimabad and Safarabad stations during 1991-2014

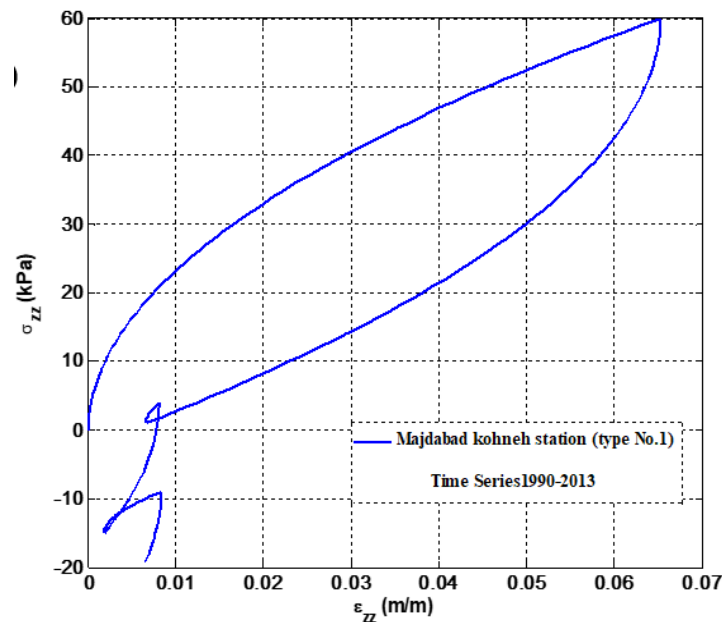


**Figure 10.** Stress-strain curve for MojedabadKohneh station during loading-unloading cycles within 1991-2014

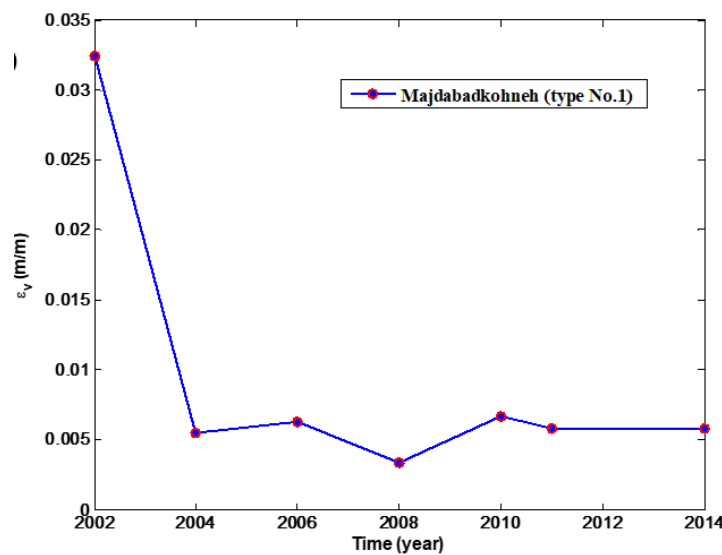


**Figure 11.** Volumetric strain rate versus time for MojedabadKohneh station during 1991-2014

In this sense, stations with gravel-based and coarse-grain soils like MojedabadKohneh have experienced more soil compaction after groundwater level drop. Another effective geotechnical characteristic in this area is the Young modulus of the local soil. Higher values of Young modulus like in Mojedabadkohneh, Safarabad and Gavkhaneh would result in higher strain rates under the same stress value. This in turn would lead to higher subsidence values.

Fig. 12 illustrates the stress-strain curve under loading-unloading cycles for the whole Arak plain during 1991-2014. It is clearly visible that over the 23-year period of investigation, the axial strain has reached extreme negative value, reducing each cycle, such that it has reached a minimum value of -0.190 in 2014. It shows severe soil compaction across the plain. The volumetric strain rate is also depicted for the plain in Fig. 13. The same trend is also visible for the volumetric strain rate. It has reached a minimum value of -0.083, which shows excessive subsidence. In case the same trends have continued over the years, the predictions show

continuing soil compaction and consequent land subsidence during previous years.

### *Land subsidence of the whole plain*

Fig. 14 shows the calculated land subsidence values for the five mentioned stations across Arak plain. By the first look, severe land subsidence is obvious across the plain, which has totally changed the topological status of the region over 1991-2014. Safarabad has approximately become the deepest section of the plain, while Gavkhaneh has undergone the maximum subsidence among the stations. Also, at Ebrahimabad station the land has somewhat inflated, while Aamanabad station has experienced a low amount of subsidence. Finally, the Majabadkohneh's land level has approximately remained the same. The land subsidence could be estimated for each region across the plain based on the depicted contour lines as the difference between the line values at each point.

It is evident from the figure that there is high potential for fine-grain compressible sedimentation due to the developed land subsidence. In fine-grain soil the hydraulic pressure would decrease by increasing the stress load higher than the normal stress due to water drainage from soil pores. This process would lead to irreversible soil compaction. While taking place gradually and over long periods of time, plastic deformations of the soil structure would follow, which would cause filling of the empty spaces within the soil medium. Consequently, the medium would undergo volume and thickness reduction and ultimate land subsidence. Considering the geotechnical structure of Arak plain aquifer and the plain's soil layering characteristics, the Young modulus would increase by increasing depth in fine-grain soil. On the other hand, due to water storage in fine-grain soil structure, the probability of ground inflation and future land subsidence is higher for fine-grain soil as compared to coarse-grain one. The presence of coarse-grain soils like gravel layers, could be beneficial for this situation due to higher water drainage rates.

The acquired results shown in Fig. 14 indicates the necessity of emergent measures for preventing further underground water exploitation and consequent land subsidence. If the overall trend of the past years continues in the future, the topology of the region will more severely change. It should be noted that topology changes and land subsidence are not defects that could be compensated and must be prevented where possible.

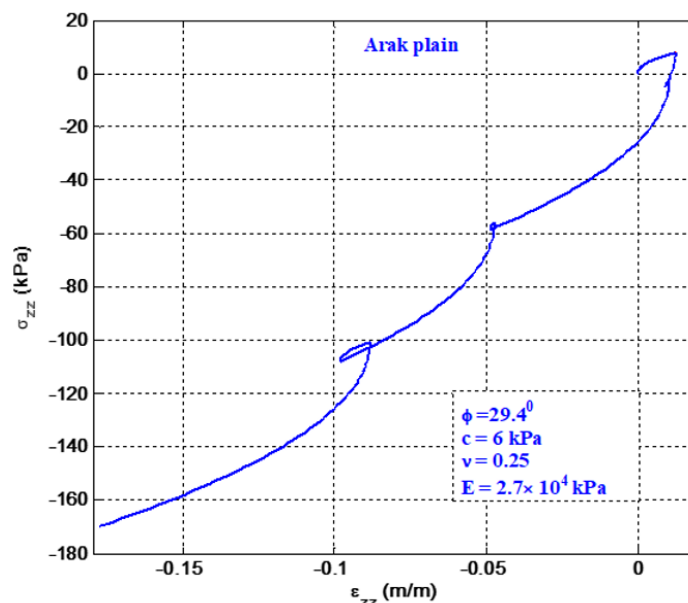


**Figure 12.** Stress-strain curve for Arak plain during loading-unloading cycles within 1991-2014

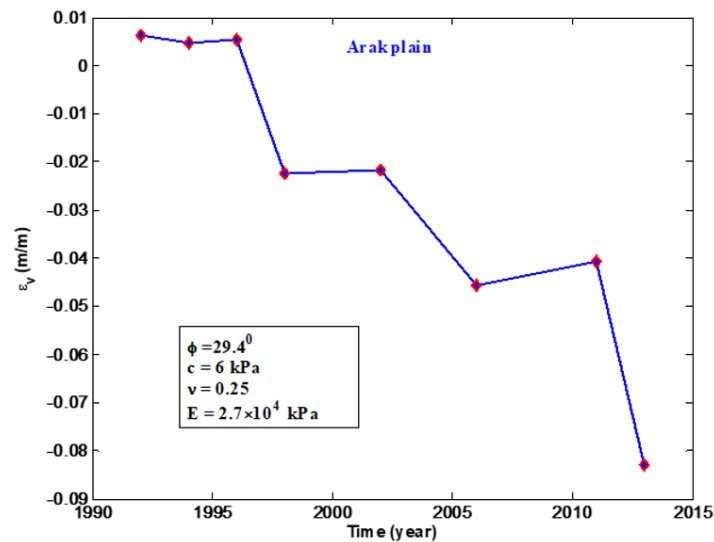


Figure 13. Volumetric strain rate for Arak plain during 1991-2014

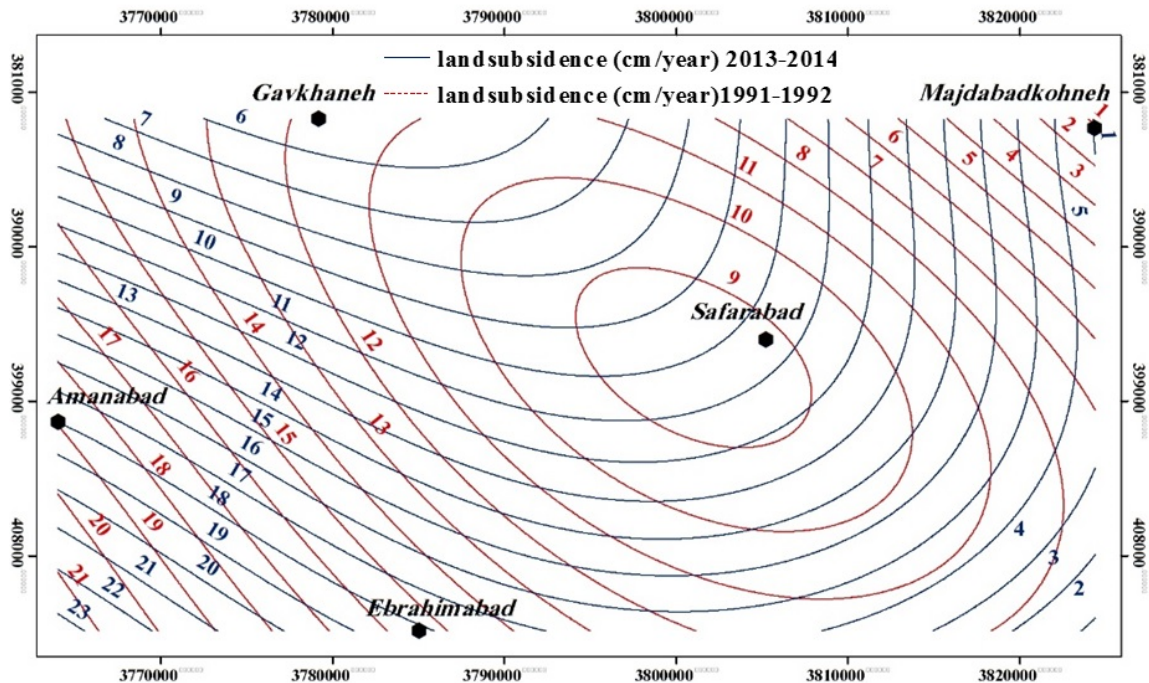


Figure 14. Contour demonstration of land subsidence in Arak plain

*Subsidence calculation using PLAXIS 2D*

Table 3 shows the defined phases for the whole plain along with input loading and water level. The calculated axial strain rate as well the subsidence value is also listed for each phase. The initial water level is assumed to be 23 m for Arak plain, according to the data acquired from regional water company of Markazi. The aggregated land subsidence was calculated as mentioned in the section 2. This value was acquired to be -11.20 cm for the whole plain. This shows a 1.03 cm difference with the previously acquired value by the Mohr-Coulomb model via loading-unloading cycles modeling, which was -10.17 cm. The difference between the output of the two methodologies equals 9.20%, which is acceptable considering the uncertainty in the measured input data.

For further analysis, the effects of underground water level and the fine-grain layer thickness were investigated on the subsidence value based on the developed FEM model. Fig. 15 shows the subsidence value versus the water level drop for an average fine-grain layer thickness across the whole plain. It is observed from the figure that as the water level drop has increased by 5 m steps, the subsidence has increased in an almost linear manner. Also, Fig. 16 shows subsidence variation with fine-grain layer thickness. It is evident that as the layer thickness was increased, the subsidence value was increased. For the minimum and maximum fine-grain layer thicknesses, subsidence values of -3.46 cm and -10.08 cm were acquired, respectively.

Finally, Fig. 17 depicts the calculated land subsidence values for measurement boreholes acquired from the FEM model versus the water level drop. For comparison, it is observed from the figure that the subsidence of Amanabad station is acquired to be 6.32 cm for 14.14 cm of water level drop. This value was acquired to be 6.48 cm calculated via the Mohr-Coulomb model, as illustrated in the previous section, which shows 2.47% of difference. Acceptable difference between the acquired results from the Mohr-Coulomb model and the FEM model, further proves the capability of the mathematical Mohr-Coulomb model for predicting land subsidence behavior for various soil aquifer structures.

**Table 3.** FEM calculation phases for Arak plain

Identification	Calculation	Loading input (kPa)	Water level (m/year)	$\epsilon_{yy}$ (m/m)	Land subsidence (cm/year)
Phase 1	plastic	-14.2	0.79	5.64E-3	1.30E-01
Phase 2	plastic	24.093	-1.34	5.78E-3	1.33E-01
Phase 3	plastic	-4.495	0.25	6.06E-3	1.39E-01
Phase 4	plastic	100.688	-5.60	6.16E-3	1.42E-01
Phase 5	plastic	-4.8546	0.27	6.23E-3	1.43E-01
Phase 6	plastic	93.496	-5.20	6.29E-3	1.45E-01
Phase 7	plastic	-12.586	0.70	6.35E-3	1.46E-01
Phase 8	plastic	124.601	-6.93	6.40E-3	1.47E-01

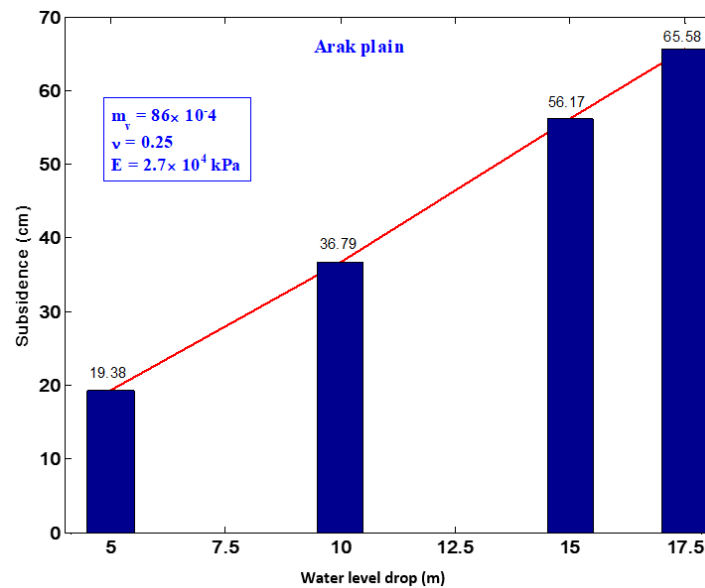


**Figure 15.** Land subsidence variation versus water level drop acquired from the FEM model for Arak plain

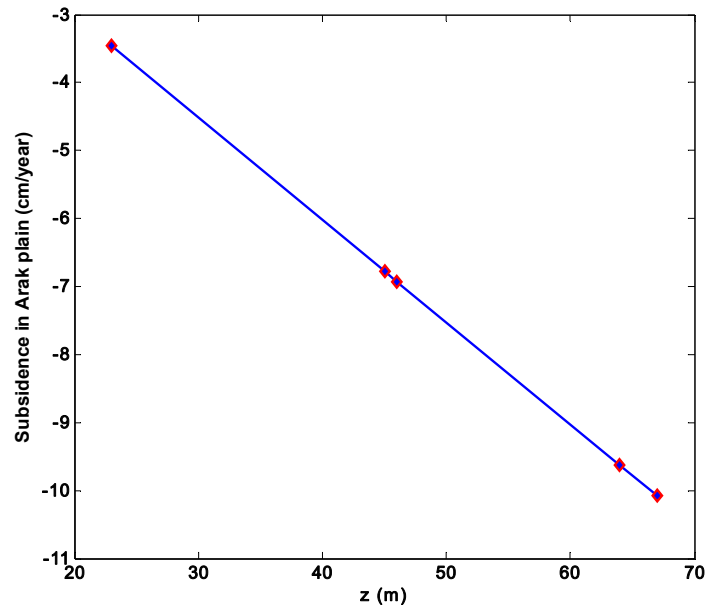


**Figure 16.** Land subsidence variations versus fine-grain layer thickness acquired from the FEM model for Arak plain

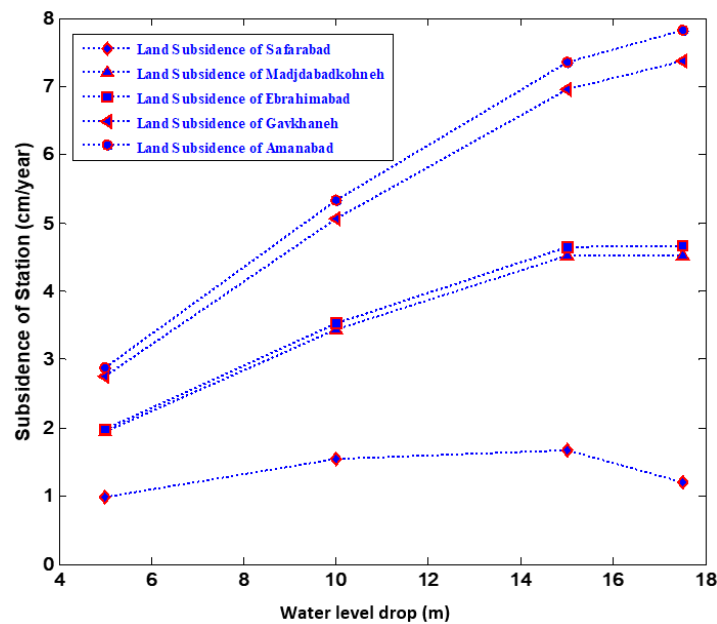


**Figure 17.** Land subsidence of measurement boreholes versus water level drop acquired from the FEM model across Arak plain

### Conclusions

Land subsidence due to groundwater overexploitation has become a major concern in the last decade throughout the world, including Iran. In this study, elastoplastic Mohr-Coulomb model is used for modeling the stress-strain behavior of soil's porous media. The acquired results for strain rate values are used for estimating the land subsidence across Arak plain within 1991-2014. For this purpose, five measurement boreholes were considered throughout the plain, namely, Gavkhaneh, Amanabad, Ebrahimabad, Mojedabadekohneh, and Safarabad. The geotechnical and stratigraphic data of each borehole were provided by regional water company

of Markazi, which were used for porous media simulation. For each station, the stress-strain as well as the volumetric strain curves were calculated and presented. These curves are also presented for the whole plain. The acquired results show a progressive soil compaction at most stations and across the whole plain, such that the axial and volumetric strains have reached minimum values of -0.190 and -0.083 in 2014. The overall trend shows progressive negative values for axial as well as volumetric strain rates at most stations and the plain, although some stations, such as MojedabadeKohneh, show approximately constant levels of strain rates.

Land subsidence values were then estimated across the plain using the axial and volumetric strain rates estimated via elastoplastic Mohr-Coulomb model. The acquired results show major variations in the region topography. Safarabad station has become the deepest region across the plain over the investigation period, while MojedabadeKohneh station has remained at the same level. The maximum subsidence is estimated to be at Gavkhaneh station and the minimum value is estimated to be at Safarabad station, being 88.75 cm and 0.2 cm, respectively. Also, it is understood that the maximum negative average subsidence takes place at Gavkhaneh station. The structure of the soil medium at the aquifer and the Young modulus showed to be determining in behavior of each station. Coarse-grain stations show lower levels of land subsidence while fine-grain mediums are more prone to irreversible land subsidence.

In the final section of the study, the subsidence behavior was also modeled using a modified FEM model via plaxis2D commercial program. In the implemented modelling, the Mohr-Coulomb model was considered to govern the stress-strain constitutive behavior of the porous medium. The acquired results from the FEM model yielded 9.20% of difference with the Mohr-Coulomb model, which further proves the capability of the latter approach in modelling land subsidence. It was also found that land subsidence has approximately a linear relation with the water level drop as well as the fine-grain layer thickness. The aggregated land subsidence value of the plain was acquired to be 26.60 cm in average. This value is concerning and in case the same trend of underground water level drop has continued over the past few years, higher values of subsidence could be predicted for the plain. This fact indicates the necessity of emergent preventive measures to be taken and groundwater exploitation levels to be controlled over the region.

## References

- Abidin, Hasanuddin Z., Rochman Djaja, Dudy Darmawan, Samsul Hadi, Arifin Akbar, H. Rajiyowiryo, Y. Sudibyo, I. Meilano, M. A. Kasuma, J. Kahar, and Cecep Subarya. 2001. "Land Subsidence of Jakarta (Indonesia) and Its Geodetic Monitoring System." *Natural Hazards* 23(2-3):365-87.
- Alipour, S., M. Motgah, M. A. Sharifi, and T. R. Walter. 2008. "InSAR Time Series Investigation of Land Subsidence Due to Groundwater Overexploitation in Tehran, Iran." *Proceedings of the 2008 2nd Workshop on USE of Remote Sensing Techniques for Monitoring Volcanoes and Seismogenic Areas, USReST 2008* (1):2-6.
- Aly, M. H., H. A. Zebker, J. R. Giardino, and A. G. Klein. 2009. "Permanent Scatterer Investigation of Land Subsidence in Greater Cairo, Egypt." *Geophysical Journal International* 178(3):1238-45.
- Anderssohn, Jan, Hans Ulrich Wetzel, Thomas R. Walter, Mahdi Motagh, Yahya Djamour, and Hermann Kaufmann. 2008. "Land Subsidence Pattern Controlled by Old Alpine Basement Faults in the Kashmar Valley, Northeast Iran: Results from InSAR and Levelling." *Geophysical Journal International* 174(1):287-94.
- Buckley, Sean M., Paul A. Rosen, Scott Hensley, and Byron D. Tapley. 2003. "Land Subsidence in Houston, Texas, Measured by Radar Interferometry and Constrained by Extensometers." *Journal of Geophysical Research* 108(B11):2542.
- Calderhead, A. I., R. Therrien, A. Rivera, R. Martel, and J. Garfias. 2011. "Simulating Pumping-Induced Regional Land Subsidence with the Use of InSAR and Field Data in the Toluca Valley, Mexico." *Advances in Water Resources* 34(1):83-97.

- Carnec, C., and H. Fabriol. 1999. "Monitoring and Modeling Land Subsidence at the Cerro Prieto Geothermal Field, Baja California, Mexico, Using SAR Interferometry." *Geophysical Research Letters* 26(9):1211-14.
- Chai, J. C., S. L. Shen, H. H. Zhu, and X. L. Zhang. 2004. "Land Subsidence Due to Groundwater Drawdown in Shanghai." *Géotechnique* 54(2):143-47.
- Chaussard, Estelle, Shimon Wdowinski, Enrique Cabral-Cano, and Falk Amelung. 2014. "Land Subsidence in Central Mexico Detected by ALOS InSAR Time-Series." *Remote Sensing of Environment* 140:94-106.
- Conway, Brian D. 2015. "Land Subsidence and Earth Fissures in South-Central and Southern Arizona, USA." *Hydrogeology Journal* 24(3):649-55.
- Dehghani, Maryam, and Mohammad Reza Nikoo. 2019. "Monitoring and Management of Land Subsidence Induced by Over-Exploitation of Groundwater." *Advances in Natural and Technological Hazards Research* 48:271-96.
- Dehghani, Maryam, Mohammad Javad Valadan Zoej, Iman Entezam, Ali Mansourian, and Sassan Saatchi. 2009. "InSAR Monitoring of Progressive Land Subsidence in Neyshabour, Northeast Iran." *Geophysical Journal International* 178(1):47-56.
- Dehghani, Maryam, Mohammad Javad Valadan Zoej, Andrew Hooper, Ramon F. Hanssen, Iman Entezam, and Sassan Saatchi. 2013. "Hybrid Conventional and Persistent Scatterer SAR Interferometry for Land Subsidence Monitoring in the Tehran Basin, Iran." *ISPRS Journal of Photogrammetry and Remote Sensing* 79:157-70.
- Fielding, Eric J., Ronald G. Blom, and Richard M. Goldstein. 1998. "Rapid Subsidence over Oil Fields Measured by SAR Interferometry." *Geophysical Research Letters* 25(17):3215-18.
- Galloway, Devin L., and Thomas J. Burbey. 2011. "Review: Regional Land Subsidence Accompanying Groundwater Extraction." *Hydrogeology Journal* 19(8):1459-86.
- Gambolati, G., and P. Teatini. 2015. "Geomechanics of Subsurface Water Withdrawal and Injection." *Water Resources Research* 51(6):3922-55.
- Gambolati, Giuseppe, Pietro Teatini, Lucio Tomasi, and Marco Gonella. 1999. "Coastline Regression of the Romagna Region, Italy, Due to Natural and Anthropogenic Land Subsidence and Sea Level Rise." *Water Resources Research* 35(1):163-84.
- Ghorbanzadeh, Omid, Hashem Rostamzadeh, Thomas Blaschke, Khalil Gholaminia, and Jagannath Aryal. 2018. "A New GIS-Based Data Mining Technique Using an Adaptive Neuro-Fuzzy Inference System (ANFIS) and k-Fold Cross-Validation Approach for Land Subsidence Susceptibility Mapping." *Natural Hazards* 94(2):497-517.
- Higgins, Stephanie, Irina Overeem, Akiko Tanaka, and James P. M. Syvitski. 2013. "Land Subsidence at Aquaculture Facilities in the Yellow River Delta, China." *Geophysical Research Letters* 40(15):3898-3902.
- Hu, R. L., Z. Q. Yue, L. C. Wang, and S. J. Wang. 2004. "Review on Current Status and Challenging Issues of Land Subsidence in China." *Engineering Geology* 76(1-2):65-77.
- Jin, Wei ze, Zu jiang Luo, and Xin hui Wu. 2016. "Sensitivity Analysis of Related Parameters in Simulation of Land Subsidence and Ground Fissures Caused by Groundwater Exploitation." *Bulletin of Engineering Geology and the Environment* 75(3):1143-56.
- Karegar, Makan A., Timothy H. Dixon, and Simon E. Engelhart. 2016. "Subsidence along the Atlantic Coast of North America: Insights from GPS and Late Holocene Relative Sea Level Data." *Geophysical Research Letters* 43:3126-33.
- Kolker, Alexander S., Mead A. Allison, and Sultan Hameed. 2011. "An Evaluation of Subsidence Rates and Sea-Level Variability in the Northern Gulf of Mexico." *Geophysical Research Letters* 38(21):1-6.
- Koster, Kay, Gilles Erkens, and Cor Zwanenburg. 2016. "A New Soil Mechanics Approach to Quantify and Predict Land Subsidence by Peat Compression." *Geophysical Research Letters* 43(20):10,792-10,799.
- Krejci, T., T. Koudelka, and M. Broucek. 2013. "Numerical Modelling of Moisture Transfer in Saturated and Non-Saturated Porous Media." *AIP Conference Proceedings* 1558(May 2014):988-91.
- Larson, K. J., H. Başağaoğlu, and M. A. Mariño. 2001. "Prediction of Optimal Safe Ground Water Yield and Land Subsidence in the Los Banos-Kettleman City Area, California, Using a Calibrated Numerical Simulation Model." *Journal of Hydrology* 242(1-2):79-102.

- Li, Changjiang, Xiaoming Tang, and Tuhua Ma. 2006. "Land Subsidence Caused by Groundwater Exploitation in the Hangzhou-Jiaxing-Huzhou Plain, China." *Hydrogeology Journal* 14(8):1652-65.
- Li, Chao, and Shao Feng Liu. 2014. "Cretaceous Anomalous Subsidence and Its Response to Dynamic Topography in the Songliao Basin, Northeast China." *Journal of Asian Earth Sciences* 109:86-99.
- Lubis, Ashar Muda, Toshinori Sato, Nobuhiro Tomiyama, Nobuhiro Isezaki, and Tsutomu Yamanokuchi. 2011. "Ground Subsidence in Semarang-Indonesia Investigated by ALOS-PALSAR Satellite SAR Interferometry." *Journal of Asian Earth Sciences* 40(5):1079-88.
- Mahmoudpour, Masoud, Mashalah Khomehchiyan, Mohammad Reza Nikudel, and Mohammad Reza Ghassemi. 2016. "Numerical Simulation and Prediction of Regional Land Subsidence Caused by Groundwater Exploitation in the Southwest Plain of Tehran, Iran." *Engineering Geology* 201(2016):6-28.
- Marfai, Muh Aris, and Lorenz King. 2007. "Monitoring Land Subsidence in Semarang, Indonesia." *Environmental Geology* 53(3):651-59.
- Motagh, Mahdi, Yahya Djamour, Thomas R. Walter, Hans Ulrich Wetzler, Jochen Zschau, and Siavash Arabi. 2007. "Land Subsidence in Mashhad Valley, Northeast Iran: Results from InSAR, Levelling and GPS." *Geophysical Journal International* 168(2):518-26.
- Ortega-Guerrer, Adrian, David L. Rudolph, and John A. Cherry. 1999. "Analysis of Long-Term Land Subsidence near Mexico City: Field Investigations and Predictive Modeling." *Water Resources Research* 35(11):3327-41.
- Ortiz-Zamora, Dalia, and Adrian Ortega-Guerrero. 2010. "Evolution of Long-Term Land Subsidence near Mexico City: Review, Field Investigations, and Predictive Simulations." *Water Resources Research* 46(1):1-15.
- Phien-wej, N., P. H. Giao, and P. Nutalaya. 2006. "Land Subsidence in Bangkok, Thailand." *Engineering Geology* 82(4):187-201.
- Rajabi, Ali M. 2018. "A Numerical Study on Land Subsidence Due to Extensive Overexploitation of Groundwater in Aliabad Plain, Qom-Iran." *Natural Hazards* 93(2):1085-1103.
- Sayyaf, M., M. Mahdavi, O. R. Barani, S. Feiznia, and B. Motamedvaziri. 2014. "Simulation of Land Subsidence Using Finite Element Method: Rafsanjan Plain Case Study." *Natural Hazards* 72(2):309-22.
- Shearer, T. R. 1998. "A Numerical Model to Calculate Land Subsidence, Applied at Hangu in China." *Engineering Geology* 49(2):85-93.
- Taravatrooy, Narges, Mohammad Reza Nikoo, Mojtaba Sadegh, and Mohammad Parvinnia. 2018. "A Hybrid Clustering-Fusion Methodology for Land Subsidence Estimation." *Natural Hazards* 94(2):905-26.
- Teatini, P., M. Ferronato, G. Gambolati, and M. Gonella. 2006. "Groundwater Pumping and Land Subsidence in the Emilia-Romagna Coastland, Italy: Modeling the Past Occurrence and the Future Trend." *Water Resources Research* 42(1):1-19.
- Tung, Hsin, and Jyr Ching Hu. 2012. "Assessments of Serious Anthropogenic Land Subsidence in Yunlin County of Central Taiwan from 1996 to 1999 by Persistent Scatterers InSAR." *Tectonophysics* 578:126-35.
- Wöppelmann, Guy, Gonéri Le Cozannet, Marcello De Michele, Daniel Raucoules, Anny Cazenave, Manuel Garcin, Susan Hanson, Marta Marcos, and Alvaro Santamaria-Gómez. 2013. "Is Land Subsidence Increasing the Exposure to Sea Level Rise in Alexandria, Egypt?" *Geophysical Research Letters* 40(12):2953-57.
- Wu, Ji Chun, Xiao Qing Shi, Shu Jun Ye, Yu Qun Xue, Yun Zhang, and Jun Yu. 2009. "Numerical Simulation of Land Subsidence Induced by Groundwater Overexploitation in Su-Xi-Chang Area, China." *Environmental Geology* 57(6):1409-21.
- Xu, Han, Xin-wen Wang, Dan-ping Yan, and Liang Qiu. 2018. "Journal of Asian Earth Sciences Subsidence Transition during the Post-Rift Stage of the Dongpu Sag, Bohai Bay Basin, NE China: A New Geodynamic Model." *Journal of Asian Earth Sciences* 158(March):186-99.
- Yang, Yong, Xian Fang Song, Fan Dong Zheng, Li Cai Liu, and Xiao Juan Qiao. 2015. "Simulation of Fully Coupled Finite Element Analysis of Nonlinear Hydraulic Properties in Land Subsidence Due to Groundwater Pumping." *Environmental Earth Sciences* 73(8):4191-99.
- Ye, Shujun, Yue Luo, Jichun Wu, Xuexin Yan, Hanmei Wang, Xun Jiao, and Pietro Teatini. 2016. "Three-Dimensional Numerical Modeling of Land Subsidence in Shanghai, China." *Hydrogeology*

- Journal 24(3):695-709.
- Zhang, Yun, Jun Yu, Xulong Gong, Jichun Wu, and Zhecheng Wang. 2018. "Pumping-Induced Stress and Strain in Aquifer Systems in Wuxi, China." *Hydrogeology Journal* 26(3):771-87.
- Zhou, Nianqing, Pieter A. Vermeer, Rongxiang Lou, Yiqun Tang, and Simin Jiang. 2010. "Numerical Simulation of Deep Foundation Pit Dewatering and Optimization of Controlling Land Subsidence." *Engineering Geology* 114(3-4):251-60.
- Zhu, Lin, Huili Gong, Xiaojuan Li, Rong Wang, Beibei Chen, Zhenxue Dai, and Pietro Teatini. 2015. "Land Subsidence Due to Groundwater Withdrawal in the Northern Beijing Plain, China." *Engineering Geology* 193:243-55.



This article is an open-access article distributed under the terms and conditions of the Creative Commons Attribution (CC-BY) license.